Hindawi
Geofluids
Volume 2021, Article ID 7225280, 10 pages
https://doi.org/10.1155/2021/7225280

Research Article

Experimental Study on the Suspension Amount of Invasion Gas in Drilling Fluid with Yield Stress

Hongtao Liu,[1,2] Yan Jin,[1] and Bing Guo[3]

[1]*School of Petroleum Engineering, China University of Petroleum (Beijing), Beijing 102249, China*
[2]*Research Institute of Oil & Gas Engineering, Tarim Oilfield, PetroChina, Kurle, Xinjiang 841000, China*
[3]*Foreign Cooperation Projects Department, Dagang Oilfield Company, Tianjin 300450, China*

Correspondence should be addressed to Yan Jin; jinycpu@126.com

Received 14 June 2021; Revised 29 August 2021; Accepted 21 September 2021; Published 11 October 2021

Academic Editor: Bailu Teng

The gas suspension phenomenon caused by the yield stress of the drilling fluid affects the accurate calculation of wellbore pressure after gas invasion. At present, most studies on the bubble suspension in the yield stress fluid focus on the single-bubble suspension condition and there are few studies on the gas suspension concentration. This paper carried out the GSC (gas suspension concentration) experiment in the simulated drilling fluid, xanthan solution, with different gas invasion methods. The GSC in the drilling fluid under the conditions of diffuse gas invasion and differential pressure gas invasion was simulated by using two methods of stir-depressurization and continuous ventilation. The results showed that when the size of a single bubble satisfied the single-bubble suspension condition, multiple bubbles can be suspended at the same time. The GSC is affected by the average size of the suspended bubbles, the yield stress of the drilling fluid, and the gas invasion modes. For different gas invasion modes, the empirical models of critical GSC related to the dimensionless number Bi are established. Compared with the experimental data, the relative error of the critical GSC in diffuse gas invasion is less than 6% and the relative error of the critical GSC in differential pressure gas invasion is less than 10%. The results of this work can provide guiding significance for accurate calculation of wellbore pressure.

1. Introduction

As oil and gas drilling continues to move towards deep fields and deep seas, complex formation conditions and temperature and pressure environments have brought great challenges to the accurate calculation and control of wellbore pressure [1, 2]. The rheology of drilling fluids is mostly Bingham [3] or Hershel-Bulkley [4] fluid. When the applied shear stress is less than the yield stress of the drilling fluid, the drilling fluid does not flow plastically. When the gas invades the wellbore, the presence of yield stress will cause the bubbles with small buoyancy to be suspended in the drilling fluid. The phenomenon of gas suspension will affect the gas distribution and migration rules in the wellbore after gas invasion, resulting in inaccurate calculation of wellbore pressure [5–7].

1.1. Single-Bubble Suspension Condition. Most of the existing researches on suspended bubbles in yield stress fluids focus on the non-Newtonian rheology of wellbore fluids [8–10], the bubble slip velocity in yield stress fluid [11, 12], and the single-bubble (or particle) suspension condition [13–16]. When a bubble is suspended in a yield stress fluid, the buoyancy causes it to move upward and its size is related to the bubble size and density difference. The velocity and shear rate of the fluid particle around the suspended bubble are both zero, and the velocity-related forces such as the viscous force and inertial force of the fluid particle are also zero. When the shape of the suspended bubble is spherical or ellipsoidal, the resultant force of the surface tension in the direction of gravity is also 0 and only the yield stress provides resistance to the bubble. Beris et al. [17] proposed the dimensionless number Bi, which is the ratio of yield

stress to buoyancy, to describe the suspension condition of a single sphere, and found that when the Bi value is greater than a certain critical value Bi_c, it will be suspended in the fluid.

$$Bi = \frac{\tau_y}{\rho g R}. \quad (1)$$

Tsamopoulos and Dimakopoulos [16, 18] obtained the Bi_c of a single spherical bubble suspended in the numerical simulation which is about 0.143, and as the aspect ratio of the suspended bubble increases, the Bi_c value gradually increases. Dubash and Frigaard [19, 20] used the variational principle to calculate the critical suspension criterion Bi_c of bubbles and conducted experiments on the critical suspension conditions of single bubbles in Carbopol solution, but compared with the experimental results, the theoretical calculation of Bi_c was too conservative. Sikorski et al. [13] conducted single-bubble critical suspension experiments in Carbopol solutions with yield stresses of 24.1 Pa and 33.5 Pa and obtained critical suspended bubble Bi_c values of 0.59 and 0.72, respectively.

Very recently, Sun et al. [21] established a bubble dynamic model for the prediction of the volume and geometry of the suspended bubbles by considering the rheological characteristics and the critical yield region around the bubble. This work realized the prediction of the shape of the suspended bubble and the critical suspension conditions in the fluid with different yield stress. The experimental data of Liu et al. [13] and Samson et al. [22] also agreed with the results calculated by the model. Due to their model results, the critical suspension conditions, Bi_c, are a function of yield stress, surface tension, and elastic modulus. This function unifies the single-bubble suspension conditions, and the Bi_c of a single spherical suspension bubble is about 0.243. This work laid a foundation for the calculation of GSC and provides a possibility for accurate prediction of wellbore pressure during gas suspension.

1.2. Suspension of Bubble Groups. Actually, most of the gas is dispersed in the drilling fluid in the form of bubble groups. When multiple bubbles in the yield stress fluid satisfy the suspension condition of a single bubble at the same time, the strain state of the liquid phase around each bubble is affected by the coupled stress field of itself and the surrounding bubbles [21]. When the distance between the bubbles is far enough, the liquid phase around a single bubble will not flow under the action of the coupled stress field, that is, multiple bubbles can remain suspended at the same time. When multiple bubbles are suspended, the total volume of gas in per unit volume is GSC.

The calculation model of the stress field around a single suspended bubble established by Sun et al. [21] shows that the farther away from the bubble center, the smaller the stress on the fluid particle. With different gas distribution characteristics, the distance between the bubbles in the wellbore is different. The coupled stress field around the bubbles is also different, resulting in differences in the concentration of the gas suspension. When the distance between multiple suspended bubbles in the drilling fluid just satisfies the condition of simultaneous suspension after gas invasion, the corresponding GSC is the critical GSC.

Johnson et al. [6] carried out an experimental study on the critical GSC during differential pressure gas invasion in a xanthan gum solution and found that the critical GSC in the solution with yield stress values of 7.2 Pa and 14.4 Pa was 0.76% and 2.47%, respectively. Considering that the bubble cannot be suspended in the yield stress fluid when the yield stress value is 0, that is, the GSC is 0. Johnson et al. [6] proposed the relationship between the critical GSC and the yield stress on the basis of two sets of experimental data, as shown in equation (2).

$$VF_c = 0.0091\tau_y^2 + 0.0405\tau_y, \quad (2)$$

where VF_c is the critical GSC, 1%.

Gas suspension is the combined effect of resistance produced by buoyancy and yield stress, and gas buoyancy is closely related to the bubble size. In the process of deep water and deep drilling, the pressure in the wellbore changes complicatedly and the bubble size is quite different [23, 24]. The suspension concentration prediction model that only considers the yield stress of the drilling fluid has poor applicability. In addition, there are only two data points in the Johnson et al. [6] model and the reliability of the model in engineering applications needs further verification.

In summary, the existing research on GSC does not consider the influence of bubble size and gas invasion mode and there are few experimental data on GSC. This paper intends to carry out experiments on the critical GSC under different gas invasion methods and establish a critical GSC prediction model considering the bubble size and distribution characteristics. In Section 2 of this article, the experimental equipment, materials, and experimental methods of the critical GSC are introduced in detail. Section 3 analyzes the influence of the suspended bubble size, yield stress, and gas invasion method on the critical GSC. In Section 4, a prediction model of critical GSC considering the yield stress of drilling fluid, bubble size, and gas invasion mode is established; Section 5 is the conclusion and discussion.

2. Critical GSC Experiment

There are different gas invasion modes in the drilling process, resulting in different distribution of bubbles in wellbore [5, 25]. When pressure difference gas invasion occurs, the gas will continue to invade the wellbore from the bottom of the well under the action of the pressure difference. During the gas rising process, part of the gas will be suspended in the wellbore. When the diffusion gas invasion occurs, the gas is dissolved into the drilling fluid driven by the concentration difference. As the drilling fluid rises, the dissolved gas gradually separates out due to the decrease in pressure. In this process, the gas is in a suspended state after being separated out. There are also differences in the distribution of gas in the wellbore in the drilling fluid under the two different gas invasion modes.

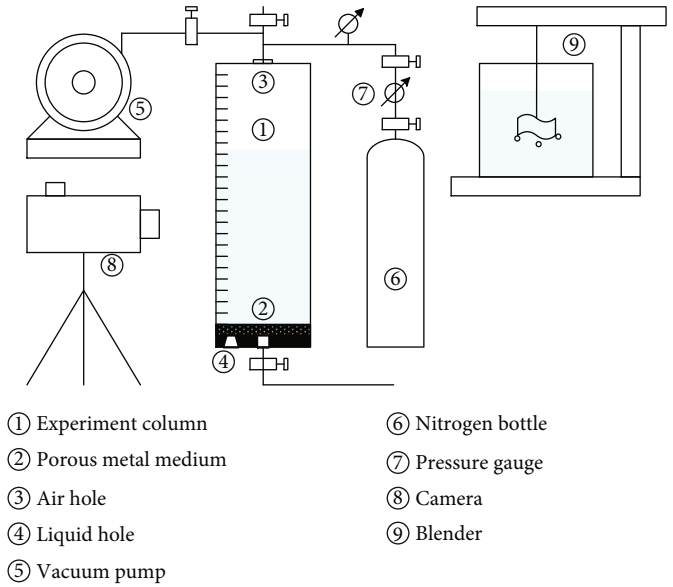

Figure 1: The schematic of the GSC apparatus.

In this work, two methods of stir-depressurization and continuous ventilation are used to simulate the conditions of diffuse gas invasion and differential pressure gas invasion, respectively, to measure the bubble size, distribution characteristics, and gas critical-suspended concentration under different gas invasion modes.

2.1. Experimental Facility. As shown in Figure 1, the experimental device for the critical GSC is composed of an experimental pipe string, a bubble generating device, a pressure control device, and a data acquisition device. The experimental column is a transparent PVC column with an inner diameter of 15 cm and a length of 120 cm. The column is sealed as a whole, and a scale line is affixed to the outside to read the height of the liquid level. The top of the column is connected to a gas cylinder, a vacuum pump, and a valve through which it is connected to the atmospheric connection. The pressure in the pipe can be controlled by adjusting the relevant valve. A small hole controlled by a valve is opened at the bottom of the pipe string for gas- and liquid-phase injection and discharge. The bubble-generating device is mainly composed of a mixer, a metal porous medium, and so on. In the stir-depressurization experiment, the gas enters the liquid phase in the form of small bubbles and dissolved gas after high-speed stirring. In the continuous ventilation experiment, gas enters the wellbore from the porous medium at the bottom. The pressure control device is mainly composed of a vacuum pump, a nitrogen cylinder, a pressure control valve, and a pressure gauge, which can adjust the pressure in the experimental column. Among them, the vacuum pump is a pressure-reducing device and the pressure in the pipe column can be reduced to 0.016 MPa at most during the experiment. The nitrogen cylinder is a pressurizing device, and the pressure in the column can be increased up to 5 MPa during the experiment. The data acquisition device is a high-speed camera, which is used to record the size and distribution of floating bubbles in the experiment.

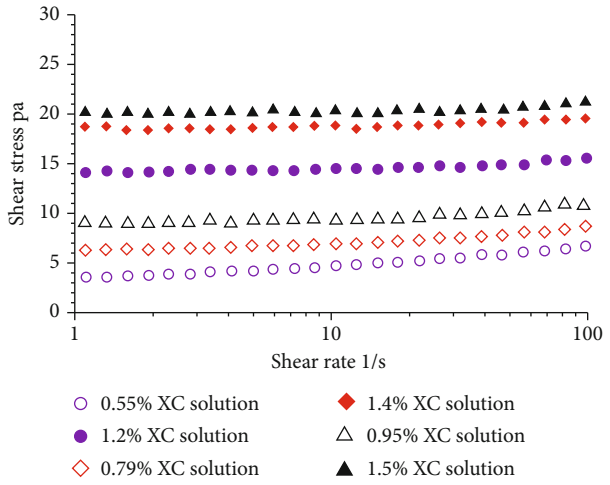

Figure 2: Rheological curve of some experimental solutions.

2.2. Experimental Materials and Properties. During the experiment, different concentrations of xanthan gum solutions were used to simulate drilling fluids with yield stress [26]. After the solution is prepared, its rheology is measured with a Physica MCR rheometer. The rheological curve of some experimental solutions is shown in Figure 2.

The rheological curve of the xanthan gum aqueous solution is in good agreement with the H-B model. The H-B model is used to fit the rheological curve data of each group of experimental solutions, and the properties of each group of experimental solutions are shown in Table 1.

2.3. Experimental Methods. The diffusion air invasion simulation experiment uses a mixer to quickly stir (500–600 rpm) to mix the air into the prepared experimental solution. After continuous stirring for 1 hour, the mixed solution was

Table 1: Rheological parameters of experimental solution.

Quality score (%)	Yield stress τ_y (Pa)	K (Pa·s^{-n})	n	Correlation coefficient R^2
0.55	2.112 ± 0.068	1.37962 ± 0.0605	0.262 ± 0.007	0.973
0.7	5.136 ± 0.029	0.46829 ± 0.022	0.416 ± 0.009	0.993
0.73	5.323 ± 0.024	0.3299 ± 0.016	0.473 ± 0.010	0.994
0.76	5.907 ± 0.022	0.27448 ± 0.014	0.499 ± 0.010	0.99935
0.79	6.029 ± 0.008	0.24194 ± 0.005	0.516 ± 0.004	0.989
0.82	7.023 ± 0.01	0.20219 ± 0.006	0.542 ± 0.006	0.978
0.87	8.165 ± 0.01	0.163 ± 0.001	0.572 ± 0.001	0.962
0.92	8.75 ± 0.002	0.125 ± 0.001	0.611 ± 0.001	0.999
0.95	8.984 ± 0.03	0.108 ± 0.002	0.633 ± 0.003	0.959
1.1	12.06 ± 0.121	0.056 ± 0.001	0.727 ± 0.002	0.948
1.2	14.16 ± 0.031	0.034 ± 0.003	0.807 ± 0.022	0.976
1.4	18.47 ± 0.09	0.017 ± 0.002	0.914 ± 0.031	0.962
1.5	20.27 ± 0.02	0.015 ± 0.001	0.919 ± 0.008	0.963

Where K is the consistency coefficient; Pa·s^{-n}: n is the flow index.

introduced into the experimental column and allowed to stand for 1 hour. The vacuum pump is used to reduce the pressure in the pipe to simulate the pressure change during the rising process of the drilling fluid containing dissolved gas.

In the experiment, the concentration of gas suspension is calculated from the height of the liquid level in the tube. After each pressure change, let it stand for 10 minutes to ensure that the bubble slippage is completed. Record the height H of the liquid level in the string under the current pressure. Use a high-speed camera to shoot the bubble size and distribution characteristics. After the pressure reaches the absolute pressure of 0.016 MPa (the maximum vacuum pressure allowed by the vacuum pump in the test), a nitrogen bottle was used to increase the pressure in the tube to about 5 MPa. After standing for 10 minutes, record the height of the liquid level in the experimental column h. The GSC is calculated in equation (3) as follows:

$$\mathrm{VF} = \frac{H - h}{H}, \tag{3}$$

where VF is the GSC.

The critical GSC is determined by the maximum value of the GSC. As the pressure decreases, the GSC of the same yield stress solution will have a maximum value. This maximum value is balanced by the increase in the bubble size caused by the pressure drop and bubble slippage. As a result, the GSC after the maximum value is the critical GSC.

$$\mathrm{VF_c} = \frac{H_{\max} - h}{H_{\max}}, \tag{4}$$

where $H_{\max}$ is the maximum liquid level recorded in the experiment.

The differential pressure gas invasion simulation experiment uses the metallic porous medium at the bottom of the experimental string to simulate the formation. The gas source gas invades the wellbore solution in the form of bubbles under the action of the pressure difference. Record the height of the liquid level in the pipe string at the initial moment as h_1. In the continuous ventilation experiment, the air source was turned off to generate bubbles after 1 hour of continuous ventilation, and the liquid level $H_{\max 1}$ in the tube was recorded 10 minutes after standing. The critical gas concentration in the experiment is

$$\mathrm{VF_c} = \frac{H_{\max\ 1} - h_1}{H_{\max\ 1}}, \tag{5}$$

where $H_{\max 1}$ is the maximum liquid level recorded during the depressurization process and h_1 is the liquid level when the pressure in the experimental column is 5 MPa.

Dubash and Frigaard [20] analyzed that when the aspect ratio of the bubble is less than 1.1, the bubble shape can be approximated as a spherical shape. The critical suspended bubbles recorded in the experiment in this paper have good axisymmetric properties, and the aspect ratio of the bubble is generally less than 1.1, so this study assumes that all suspended bubbles are spherical bubbles.

Because there is a critical suspension condition for a single bubble in the yield stress fluid, a maximum value of the suspended bubble volume is observed in the experiment, as shown in Figure 3.

When calculating the volume of floating bubbles, the IPP software was used to process the experimental photos taken by the high-speed camera and record the volume of the bubbles in the shooting area as V_i and the probability of occurrence of bubbles of this size P_i. The experiment uses the volume average particle size in the particle size analysis to

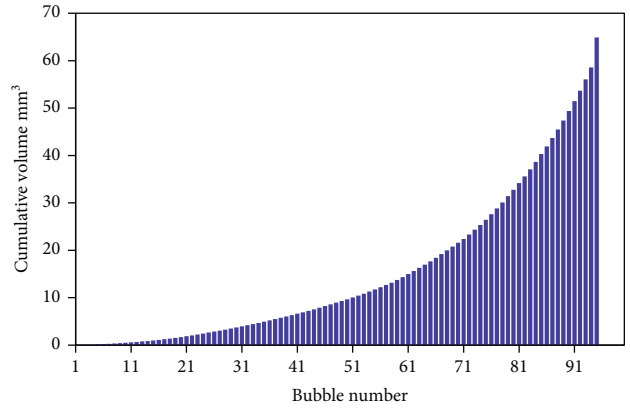

Figure 3: Cumulative volume of bubbles (xanthan gum aqueous solution, 0.76%, 0.05 Mpa).

characterize the average bubble size, and the bubble size corresponding to the average bubble volume is used as the average bubble size.

$$R_{\text{eff}} = \sqrt[3]{\sum_{i=1}^{N} \frac{3V_i P_i}{4\pi}}, \tag{6}$$

where R_{eff} is the average bubble radius of the bubble group.

3. Experimental Result

3.1. Effect of the Bubble Size on Critical Suspension Concentration. Suspended bubbles are mainly affected by buoyancy, yield stress, gas-liquid interface pressure difference, and surface tension [26]. With the decrease of the pressure in the experimental column, the liquid pressure outside the gas-liquid interface of the suspended bubble decreases, the pressure difference between the inside and outside of the gas-liquid interface increases, and the gas-liquid interface expands under the pressure in the bubble. During the bubble expansion, the pressure inside the bubble decreases gradually until the pressure difference at the gas-liquid interface is again balanced with the surface tension and the fluid shear stress (yield stress and viscous force).

As shown in Figure 4, the diameter of bubbles entering the solution at the initial moment of stirring in the solution ranged from 0 to 2.75 mm and most of the bubble diameters were concentrated in the range of 0.5–2 mm. As the pressure in the experimental column decreases, the size of the tiny bubbles entering the agitation increases, resulting in an increase in the size of 0–0.5 mm bubbles in the total volume of suspended bubbles. The average size of bubbles in the column gradually increases, and the proportion of bubbles in the total suspended gas volume in the diameter range of 0–2 mm decreases; the size of large bubbles increases.

The average diameter of suspended bubbles increases with the decrease of pressure in the column, and the suspended gas concentration changes accordingly. As shown in Figure 5, when the yield stress was the same, the GSC in the solution first increased and then decreased with the decrease of the pressure in the column. With the decrease

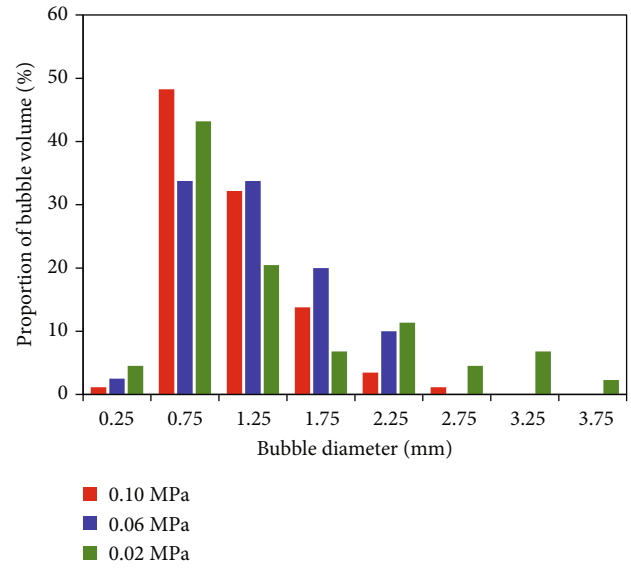

Figure 4: Bubble size distribution during depressurization (τ_y = 5.907 Pa).

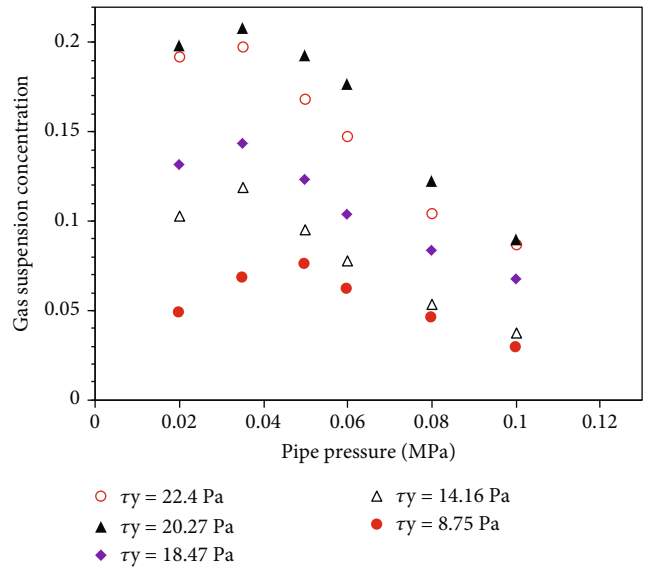

Figure 5: Pressure and GSC (xanthan glue solution).

of the pressure in the column, the volume of the suspended bubble increases and the pressure difference between the inside and the outside of the gas-liquid interface reaches equilibrium again under the action of fluid resistance. When the volume of the suspended bubble is small and the stress state of the surrounding fluid still satisfies the condition of no yield flow, the bubble will not slip and rise, that is, it will continue to suspend in the yield stress solution. At this time, the suspension concentration of gas increases with the expansion.

With the experimental pressure further reduced in the column, the bubble volume will increases and finally exceed a certain size. The yield stress is not large enough to keep the bubble being suspended. Then the bubbles will slip, which

makes the GSC decrease with increasing bubble volume. When the volume of the bubble increased because the expansion is equal to the volume decreased due to slippage, the concentration of the suspended gas reaches the limit.

The experimental results show that the size of the suspended bubble is an important factor affecting the suspended bubble concentration and the GSC prediction model without considering the bubble size cannot accurately describe the gas suspension characteristics in the wellbore after gas invasion.

3.2. Effect of Yield Stress on Critical Suspension Concentration. In addition to bubble size, the yield stress is also an important factor affecting the GSC. As shown in Figure 6, in the solution with higher yield stress, the suspended bubbles require greater buoyancy to overcome the resistance generated by the yield stress, so the size distribution range of the suspended bubbles is larger.

In the process of pressure reduction in the column, there is a finite range of bubble size in the process of bubble expansion. When the average size of suspended bubbles is relatively close, the ultimate suspension concentration of gas in solution under different yield stresses is shown in Figure 7. According to the critical suspension condition of a single bubble, when the yield stress value is constant, there exists a critical suspended bubble size, and when the bubble volume is close to this critical size, the GSC is 0. When the bubble size is close to and does not exceed the critical suspension condition of a single bubble, the larger the yield stress is, the stronger the ability to restrain the flow trend of fluid particles under the bubble coupling stress field is, that is, the closer the distance between suspended bubbles is allowed. Therefore, the larger the yield stress, the higher the GSC.

3.3. Effect of the Gas Invasion Mode on Critical Suspension Concentration. The experimental results show that the influence factors of GSC are similar to the critical suspension conditions of a single bubble, that is, they are affected by both bubble size and fluid yield stress. In addition, the critical suspension condition of a single bubble is also an important factor affecting the GSC. Therefore, the dimensionless number Bi, which can characterize both the yield stress and the gas size, is introduced to describe the variation of gas concentration. The GSC under the two different gas invasion modes is shown in Figure 8.

As can be seen in Figure 8, in the process of stirring and depressurization, when the dimensionless number Bi value is less than Bi_c corresponding to the critical suspension volume of a single bubble, the suspended gas concentration in the column is zero. With the increase of the Bi value, the suspended gas concentration obtained by stirring and depressurization gradually increased. The maximum suspended gas concentration observed in the experiment reached 20.67% and stabilized around this value. The variation law of GSC with Bi in the continuous ventilation experiment is quite different from that in the stir-depressurization experiment. In the continuous ventilation experiment, the GSC increased to the peak value (about 5.37%) and then

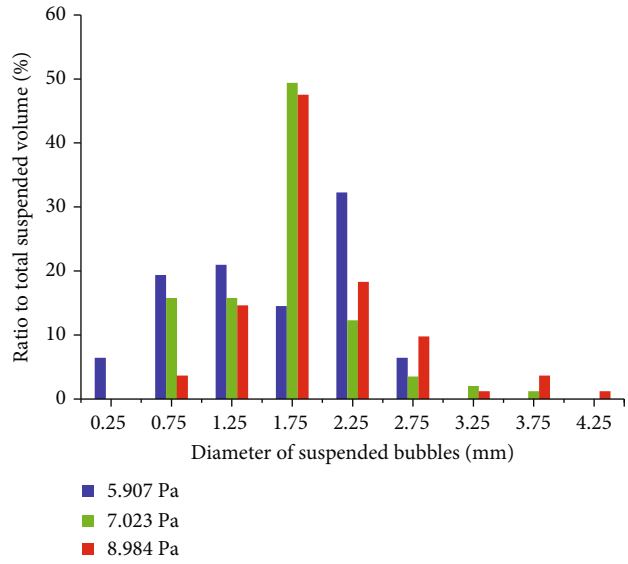

Figure 6: Yield stress and bubble size distribution (xanthan glue solution, 0.035 MPa).

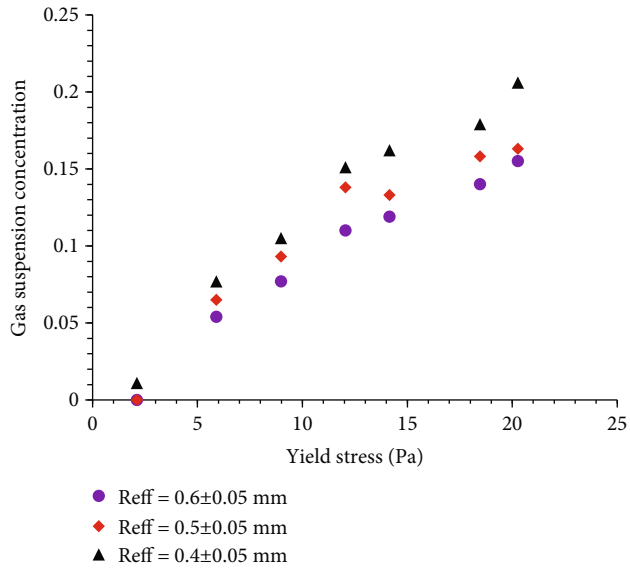

Figure 7: Variation of bubble suspension concentration with yield stress.

decreased gradually. The GSC of the two different gas invasion modes is nearly the same at Bi ranging from 1 to 1.05.

The results show that the range and peak values of Bi recorded in the continuous ventilation experiment are smaller than those in the stir-depressurization experiment. The reason is that the gas slippage affects the distribution of suspended bubbles in the continuous ventilation experiment. As shown in Figure 9, the bubbles are closely distributed in the experimental column in the stir-depressurization experiment and the GSC is only affected by the buoyancy and yield stress of the suspended bubbles. In the continuous ventilation experiment, due to a large amount of gas slipping

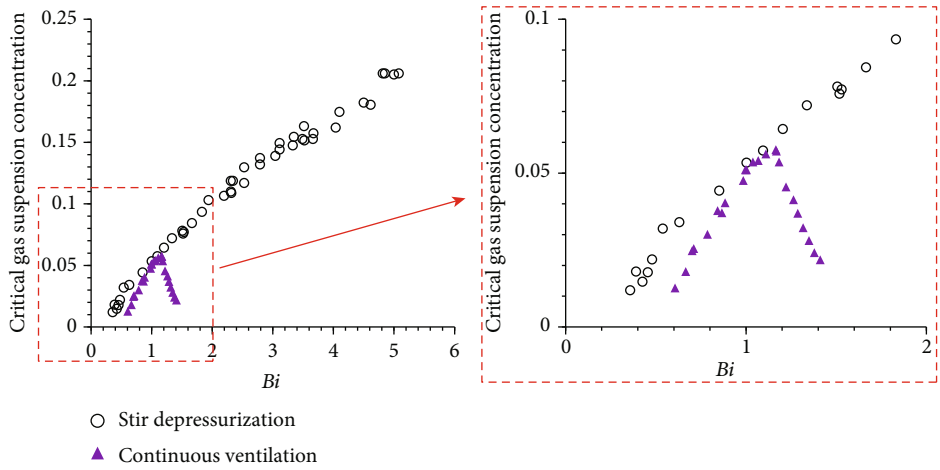

Figure 8: The critical suspension concentration under different gas invasion modes.

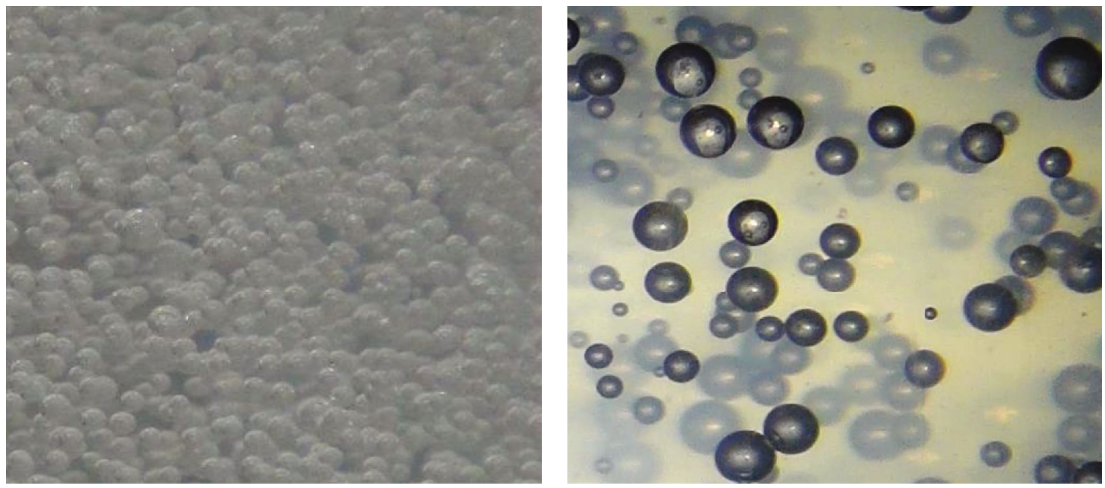

(a) Stir-depressurization experiment

(b) Continuous ventilation experiment

Figure 9: Distribution pattern of suspended bubbles under different gas invasion modes.

from the bottom of the column and rising to the liquid level, some suspended bubbles will be carried to rise above the liquid level, which will affect the GSC in the column. In addition, most of the suspended bubbles are located between the sliding and rising tracks of the moving bubbles, which leads to a larger distance between the suspended bubbles than in the stir-depressurization experiment and leads to a lower concentration of gas suspension than in the stir-depressurization experiment.

In the continuous ventilation experiment, the distance between suspended bubbles is composed of the distance between the suspended bubble and the trajectory of the migrating bubble and the diameter of the migrating bubble trajectory. The smaller the Bi value of the suspended bubble is, the closer its volume is to the critical suspended bubble volume and the stress field around the suspension is more prone to the plastic flow under the disturbance of the transporting bubble. When the allowable distance between the suspended bubble and the trajectory of the moving bubble is large enough [27–29], the suspension can be maintained. Then, with the increase of the Bi value, the stronger the anti-disturbance ability of the fluid around the suspended bubble, the smaller the allowable distance between the suspended bubble and the trajectory of the moving bubble and the smaller the distance between the bubble groups at this time. The distance between the suspended bubbles increases with the Bi value. When the Bi value increases further, the volume ratio between the suspended volume and the migrating bubble becomes smaller and the trajectory of the migrating bubble becomes larger. The influence on the distance between the suspended bubbles exceeds the influence on the reduction of the fluid stress around the suspended bubble. The actual distance between the bubbles will increase, and the GSC will decrease with the increase of Bi.

When the fluid yield stress is larger in the experiment, the bubble group generated at the bottom of the well during the continuous ventilation process is easy to gather and form larger bubbles. The disturbance of the surrounding fluid area

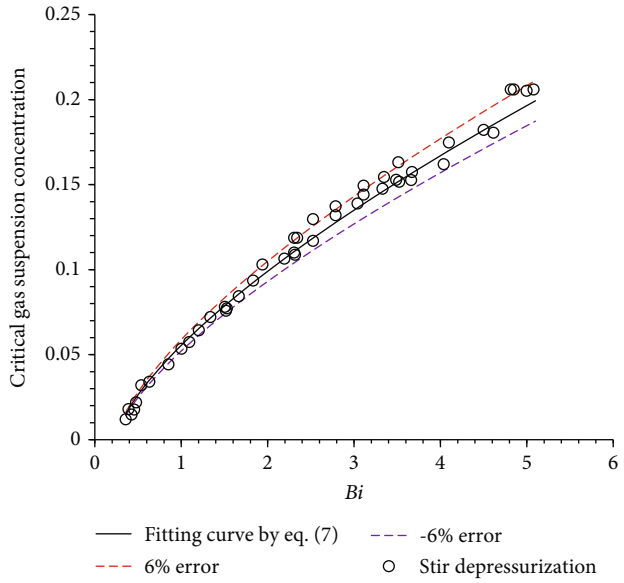

Figure 10: Prediction model of critical GSC during diffusion gas invasion.

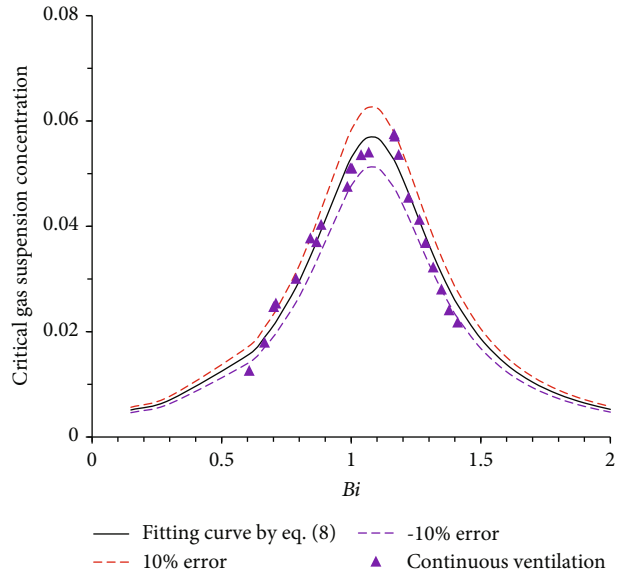

Figure 11: Prediction model of critical GSC during differential pressure gas invasion.

in the process of large bubble slipping leads to a greater distance between suspended bubbles [29], resulting in a decrease in GSC.

It can be seen that the way of gas invasion is also an important factor affecting the concentration of gas suspension.

4. Prediction Models of Critical GSC under Different Gas Invasion Modes

Considering the influence of bubble size, fluid yield stress, and gas invasion method on GSC, this paper establishes a GSC prediction model for different gas invasion methods based on the experimental results. Within the effective range of the model, it can provide a calculation basis for the calculation of gas-liquid two-phase flow in the wellbore after gas invasion.

4.1. Prediction Model of Critical GSC during Diffusion Gas Invasion. The GSC model of diffusion gas invasion (in the stirring and depressurization experiment) is shown in equation (7). When a single gas cannot be kept in suspension, the GSC is zero. When the arrangement of the bubbles reaches the tightest state, the GSC reaches the peak value. In the experiment, it is observed that the GSC peak occurs at a Bi value of about 5 and the peak value is about 20.67%. As shown in Figure 10, the model prediction results have an error of less than 6% compared with the experimental results.

$$\mathrm{VF_c} = \begin{cases} 0.0672(\mathrm{Bi} - \mathrm{Bi_c})^{0.6878}, & \mathrm{Bi_c} < \mathrm{Bi} < 5, \\ 0.2067, & \mathrm{Bi} > 5. \end{cases} \tag{7}$$

4.2. Prediction Model of Critical GSC during Differential Pressure Gas Invasion. The GSC model of differential pressure gas invasion (continuous ventilation experiment) is shown in equation (8). When a single bubble cannot be kept in suspension, the GSC is zero. When the Bi value is about 1.1, the GSC reaches the peak value and the peak value of the GSC is about 5.76% observed in the experiment. As shown in Figure 11, the model prediction results have an error of less than 10% compared with the experimental results.

$$\mathrm{VF_c} = \frac{0.0062}{1 - 2.1274(\mathrm{Bi} - \mathrm{Bi_c}) + 1.2695(\mathrm{Bi} - \mathrm{Bi_c})^2}, \quad \mathrm{Bi_c} < \mathrm{Bi} < 1.5. \tag{8}$$

5. Conclusion

In this paper, stir-depressurization and continuous ventilation experiments are used to simulate the diffusion gas invasion and differential pressure gas invasion during the drilling process. Based on the experimental results, we present the following conclusions:

(1) The critical GSC of gas in the diffusion gas invasion increases with the increase of the dimensionless number Bi, until it reaches the peak value. The critical GSC in the differential pressure gas invasion first increases and then decreases with the increase of the dimensionless number Bi

(2) The peak value of critical GSC in diffusion gas invasion is about 20.67%, and the peak value of differential pressure in gas invasion is about 5.67%

(3) Predictive models for critical GSC are established by considering the average size of suspended bubbles, the yield stress of drilling fluid, and gas invasion modes. Compared with the experimental results,

the relative error of the model that predicted critical GSC in diffusion gas invasion is less than 6% and the prediction model error of the critical GSC in differential pressure gas invasion is less than 10%

Data Availability

The data used in this job was given in the manuscript.

Conflicts of Interest

The authors declare that they have no conflicts of interest.

Acknowledgments

The authors are indebted to China University of Petroleum (Beijing) and Tarim Oilfield, PetroChina.

References

[1] B. Sun, P. Gong, and Z. Wang, "Simulation of gas kick with high H2S content in deep well," *Journal of Hydrodynamics*, vol. 25, no. 2, pp. 264–273, 2013.

[2] Z. Wang, B. Sun, X. Wang, and Z. N. Zhang, "Prediction of natural gas hydrate formation region in wellbore during deep-water gas well testing," *Journal of Hydrodynamics*, vol. 26, no. 4, pp. 568–576, 2014.

[3] E. C. Bingham, *Fluidity and Plasticity*, McGraw-Hill, 1922.

[4] W. M. Hershel and R. Bulkley, "Measurement of consistency as applied to rubber-benzene solutions," *Proceedings American Society for Testing and Materials*, vol. 26, pp. 621–634, 1926.

[5] S. Pan, B. Sun, Z. Wang et al., "A new model to improve the accuracy of wellbore pressure calculation by considering gas entrapment," in *SPE/IATMI Asia Pacific Oil & Gas Conference and Exhibition*, Bali, Indonesia, 2019.

[6] A. Johnson, I. Rezmer-Cooper, and T. Bailey, "Gas migration: fast, slow or stopped," in *SPE/IADC Drilling Conference*, Bali, Indonesia, 1995.

[7] J. Song, M. Caggioni, T. M. Squires, J. F. Gilchrist, S. W. Prescott, and P. T. Spicer, "Heterogeneity, suspension, and yielding in sparse microfibrous cellulose gels 1. Bubble rheometer studies," *Rheologica Acta*, vol. 58, no. 5, pp. 217–229, 2019.

[8] W. Fu, Z. Wang, L. Chen, and B. Sun, "Experimental investigation of methane hydrate formation in the carboxmethylcellulose (CMC) aqueous solution," *SPE Journal*, vol. 25, no. 3, pp. 1042–1056, 2020.

[9] W. Fu, Z. Wang, B. Sun, J. Xu, L. Chen, and X. Wang, "Rheological properties of methane hydrate slurry in the presence of xanthan gum," *SPE Journal*, vol. 25, no. 5, pp. 2341–2352, 2020.

[10] W. Fu, Z. Wang, J. Zhang, Y. Cao, and B. Sun, "Investigation of rheological properties of methane hydrate slurry with carboxmethylcellulose," *Journal of Petroleum Science and Engineering*, vol. 184, article 106504, 2020.

[11] W. Lou, Z. Wang, S. Pan, B. Sun, J. Zhang, and W. Chen, "Prediction model and energy dissipation analysis of Taylor bubble rise velocity in yield stress fluid," *Chemical Engineering Journal*, vol. 396, article 125261, 2020.

[12] Z. Wang, W. Lou, B. Sun, S. Pan, X. Zhao, and H. Liu, "A model for predicting bubble velocity in yield stress fluid at low Reynolds number," *Chemical Engineering Science*, vol. 201, pp. 325–338, 2019.

[13] Z. Liu, B. Sun, Z. Wang, J. Zhang, and X. Wang, "Prediction and management of hydrate reformation risk in pipelines during offshore gas hydrate development by depressurization," *Fuel*, vol. 291, article 120116, 2021.

[14] D. Sikorski, H. Tabuteau, and J. R. de Bruyn, "Motion and shape of bubbles rising through a yield-stress fluid," *Journal of Non-Newtonian Fluid Mechanics*, vol. 159, no. 1-3, pp. 10–16, 2009.

[15] Y. Dimakopoulos, M. Pavlidis, and J. Tsamopoulos, "Steady bubble rise in Herschel-Bulkley fluids and comparison of predictions via the augmented Lagrangian method with those via the Papanastasiou model," *Journal of Non-Newtonian Fluid Mechanics*, vol. 200, no. 20, pp. 34–51, 2013.

[16] J. Papaioannou, A. Giannousakis, Y. Dimakopoulos, and J. Tsamopoulos, "Bubble deformation and growth inside viscoelastic filaments undergoing very large extensions," *Industrial & Engineering Chemistry Research*, vol. 53, no. 18, pp. 7548–7569, 2014.

[17] A. N. Beris, J. A. Tsamopoulos, R. C. Armstrong, and R. A. Brown, "Creeping motion of a sphere through a Bingham plastic," *Journal of Non-Newtonian Fluid Mechanics*, vol. 158, pp. 219–244, 1985.

[18] J. Tsamopoulos, Y. Dimakopoulos, N. Chatzidai, G. Karapetsas, and M. Pavlidis, "Steady bubble rise and deformation in Newtonian and viscoplastic fluids and conditions for bubble entrapment," *Journal of Fluid Mechanics*, vol. 601, pp. 123–164, 2008.

[19] N. Dubash and I. A. Frigaard, "Conditions for static bubbles in viscoplastic fluids," *Physics of Fluids*, vol. 16, no. 12, pp. 4319–4330, 2004.

[20] N. Dubash and I. A. Frigaard, "Propagation and stopping of air bubbles in Carbopol solutions," *Journal of Non-Newtonian Fluid Mechanics*, vol. 142, no. 1-3, pp. 123–134, 2007.

[21] B. Sun, S. Pan, J. Zhang, X. Zhao, Y. Zhao, and Z. Wang, "A dynamic model for predicting the geometry of bubble entrapped in yield stress fluid," *Chemical Engineering Journal*, vol. 391, article 123569, 2020.

[22] G. Samson, A. Phelipot-Mardelé, C. Lanos, and A. Pierre, "Quasi-static bubble in a yield stress fluid: elasto-plastic model," *Rheologica Acta*, vol. 56, no. 5, pp. 431–443, 2017.

[23] J. Wang, B. Sun, W. Chen, J. Xu, and Z. Wang, "Calculation model of unsteady temperature-pressure fields in wellbores and fractures of supercritical CO_2 fracturing," *Fuel*, vol. 253, pp. 1168–1183, 2019.

[24] D. Carvajal, C. Carlesi, V. Meléndez-Vejar, D. Vásquez-Sandoval, A. H. A. Monteverde-Videla, and S. Bensaid, "Numerical simulation of single-bubble dynamics in high-viscosity ionic liquids using the level-set method," *Chemical Engineering & Technology*, vol. 38, no. 3, pp. 473–481, 2015.

[25] B. Yin, Y. Lin, Z. Wang et al., "A gas kick early detection method outside riser based on Doppler ultrasonic wave during deepwater drilling," *Petroleum Exploration and Development*, vol. 47, no. 4, pp. 846–854, 2020.

[26] E. Ong, S. O'Byrne, and J. L. Liow, "Yield stress measurement of a thixotropic colloid," *Rheologica Acta*, vol. 58, no. 6-7, pp. 383–401, 2019.

[27] A. Margaritis, D. W. te Bokkel, and D. G. Karamanev, "Bubble rise velocities and drag coefficients in non-Newtonian polysaccharide solutions," *Biotechnology and Bioengineering*, vol. 64, no. 3, pp. 257–266, 1999.

[28] W. L. Lloyd, M. D. Andrea, and J. R. Kozicz, "New considerations for handling gas in a deepwater riser," *Journal of Petroleum Technology*, vol. 53, no. 1, pp. 31-32, 2001.

[29] S. Das, L. D. Weerasiri, and W. Yang, "Influence of surface tension on bubble nucleation, formation and onset of sliding," *Colloids and Surfaces A: Physicochemical and Engineering Aspects*, vol. 516, pp. 23–31, 2017.